

# Domain-Decomposition Method for Time-Harmonic Aeroacoustic Problems

Romeo F. Susan-Resiga\* and Hafiz M. Atassi†  
*University of Notre Dame, Notre Dame, Indiana 46556*

A domain-decomposition (DD) method is developed for parallel computation of time-harmonic aerodynamic-aeroacoustic problems. The computational domain is decomposed into subdomains, and the aerodynamic-aeroacoustic boundary-value problem is solved independently for each subdomain. Impedance-type transmission conditions are imposed on the artificially introduced subdomain boundaries to ensure the uniqueness of the solution. A Dirichlet-to-Neumann map is used as a nonreflecting radiation condition along the outer computational boundary. Subdomain problems are then solved using the finite element method, and an iterative scheme updates the transmission conditions to recover the global solution. The present algorithm is implemented for two model problems. First, the sound radiated from a surface simulating a two-dimensional monopole is calculated using an unstructured mesh. Second, the flow about a thin airfoil in a transverse gust is computed using a structured mesh. The accuracy of the numerical scheme is validated by comparison with existing solutions for both the near-field unsteady pressure and the far-field radiated sound. The convergence and the computational time and memory requirements of the present method are studied. It is shown that by combining the subdomain direct solvers with global iterations this DD method significantly reduces both the computational time and memory requirements.

## I. Introduction

ACCURATE computation of aeroacoustics phenomena must preserve the wave form with minimum dispersion and dissipation. This requires a large number of grid points per wavelength throughout the computational domain. As a result, for time-harmonic waves the discrete form of the corresponding elliptic boundary-value problem usually leads to a very large system of equations.

There are two types of solvers for large system of equations, direct solvers and iterative solvers. Direct solvers are robust, but for aeroacoustic applications their memory and CPU time requirements limit their use in three-dimensional and/or high-frequency computations. Iterative solvers, on the other hand, have less memory requirements; however, their convergence rate strongly depends on the wave number, and in some instances they may not converge at all.

This paper presents a method for solving time-harmonic aerodynamic and aeroacoustic problems using domain decomposition (DD). The method has been developed for the exterior Helmholtz problem by Susan-Resiga and Atassi.<sup>1</sup> The computational domain is divided into subdomains, and the boundary-value problem is formulated and solved independently for each subdomain. On the artificially introduced subdomain boundaries, transmission conditions that ensure the uniqueness of the solution are imposed. An iterative scheme updates the transmission conditions after every iteration until the global solution is recovered. Thus, the problem can be solved concurrently in all subdomains on parallel computers. The main advantage of the present method is to reduce memory requirements for solving large systems of linear equations. Moreover, with parallel computing the computational time is also significantly reduced. The method thus provides an efficient and robust scheme for solving large systems of linear algebraic equations.

In the present paper the DD method is implemented for two model problems. First, sound radiated from a surface simulating a two-

dimensional monopole is calculated using the finite element method on unstructured mesh. This model problem is an extension to that developed in Ref. 1 for a structured mesh. A nonoverlapping mesh partitioning is used to build an overlapping domain decomposition. The algorithm also defines the new subdomain boundaries, other than the original boundaries of the global computational domain, on which transmission conditions are imposed.

Second, the unsteady flow about a thin airfoil in a transverse gust is computed to determine both the near-field unsteady pressure along the airfoil surface and the far-field radiated sound. The problem is formulated in terms of the unsteady linearized Euler equations, with the unsteady pressure as the unknown variable. This has the advantage of avoiding the velocity discontinuity in the wake and leads to a simple formulation for the radiation condition on the outer computational boundary. It also tests the accuracy of the present DD method for treating singularities such as the airfoil leading-edge singularity.

The present method uses an exact nonreflecting radiation condition based on a Dirichlet-to-Neumann map. The support of the kernel of the map is truncated to enhance the efficiency of the computations. The finite element (FE) method is used to discretize the boundary-value problem in each case. The flux associated with each subdomain interface node is used for implementing the transmission conditions. The accuracy of the numerical scheme has been validated by comparison with the exact analytical solution for the monopole problem and with the results of Atassi et al.<sup>2</sup> for both the near-field unsteady pressure along the airfoil surface and the far-field acoustic pressure.

Finally, the performance of the DD method is examined. The dependence of the convergence rate on the domain overlap and on the problem parameters (the Mach number and the reduced frequency) is investigated. The benefits of using DD for computational time and memory requirements are compared with a direct solver for the whole computational domain. It is also shown that, because of the limited communication between subdomains, the DD algorithm is particularly suitable for parallel computing.

## II. Formulation

The Helmholtz equation is the basic equation for time-harmonic waves. It also represents, through a transformation, the linearized Euler equations about a uniform mean flow.<sup>3</sup> We therefore consider the Helmholtz equation for the development and application of our DD approach.

Let us consider an infinite domain exterior to an inner boundary  $\Gamma$ , as shown in Fig. 1a. The outward unit vector normal to  $\Gamma$  is denoted

Presented as Paper 99-0355 at the 37th Aerospace Sciences Meeting, Reno, NV, 11–14 January 1999; received 7 October 1999; revision received 20 July 2000; accepted for publication 2 August 2000. Copyright © 2000 by the American Institute of Aeronautics and Astronautics, Inc. All rights reserved.

\*Postdoctoral Research Associate, Department of Aerospace and Mechanical Engineering.

†Viola D. Hank Professor, Department of Aerospace and Mechanical Engineering, Fellow AIAA.

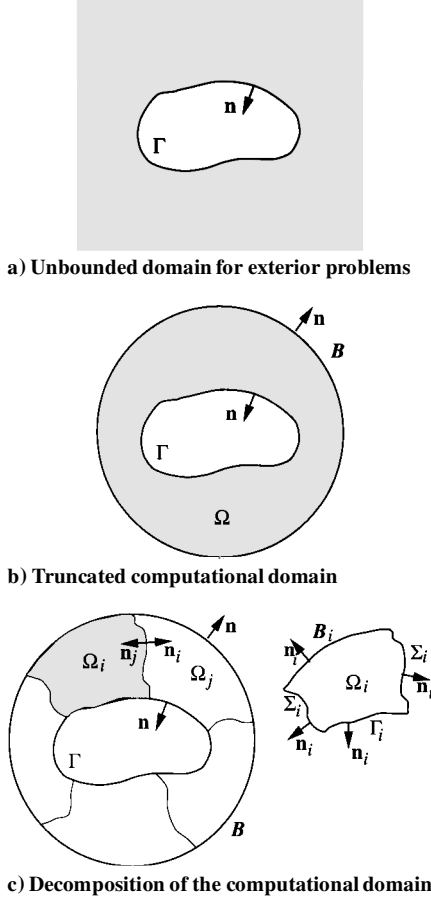


Fig. 1 Domain-based approach for exterior problems.

by  $\mathbf{n}$ . For harmonic-time dependence of the form  $u(\mathbf{x}) \exp(i\omega t)$ , the wave equation reduces to the Helmholtz equation

$$\nabla^2 u + k^2 u = 0 \quad \text{outside } \Gamma \quad (1)$$

The boundary conditions for exterior problems are defined by

$$u = f \quad \text{on } \Gamma_D \quad (2)$$

$$\frac{\partial u}{\partial n} = g \quad \text{on } \Gamma_N \quad (3)$$

$$\lim_{r \rightarrow \infty} r^{(d-1)/2} \left( \frac{\partial u}{\partial r} + iku \right) = 0 \quad (4)$$

where  $k$  is the wave number,  $\Gamma_D \cup \Gamma_N = \Gamma$ ,  $\Gamma_D \cap \Gamma_N = \emptyset$ ,  $i = \sqrt{-1}$ ,  $r$  is the distance measured from one point (origin) at a finite distance from  $\Gamma$ , and  $d = 2$  or  $3$  is the space dimension. The Sommerfeld radiation condition (4) expresses the causality principle and thus allows only solutions with outgoing waves at infinity.

There are two main approaches to solve numerically the boundary-value problem (1–4). First, one can define an equivalent problem using an integral equation formulation on the physical boundary  $\Gamma$  and solve it using the boundary element method (BEM). Second, one can introduce a computational outer boundary  $B$  and solve the problem in the bounded domain  $\Omega$  (Fig. 1b). The finite element method (FEM) can be used to discretize the boundary-value problem in the second case.<sup>4</sup> Nonreflecting conditions must be introduced along  $B$ , which essentially bring the Sommerfeld condition (4) from infinity to a finite distance.

Let us briefly examine the memory requirements for the discretized problems obtained in the two approaches. To this end, we consider a two-dimensional computational domain (Fig. 2) bounded by an ellipse  $\Gamma$  and a circle  $B$ . If the inner boundary is discretized with 200 points, the BEM leads to a system of 200 equations with a dense matrix having 40,000 entries. On the other hand, a FEM discretization with quadratic triangular elements and the same number

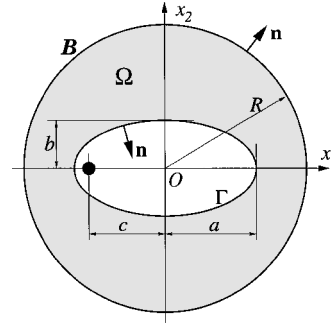


Fig. 2 Model problem: radiating monopole.

of points on the ellipse leads to a system of 3371 equations, having a sparse matrix with 41,649 nonzero entries. One can conclude that both the boundary-integral and the domain-based approaches have practically the same memory requirements, provided that the outer boundary  $B$  is close enough to  $\Gamma$ . Harari and Hughes<sup>5</sup> studied and compared the cost of obtaining solutions to problems governed by the Helmholtz equation in both interior and exterior domains by means of BEM and FEM. They found that, despite the fact that BEM needs less equations to discretize the same physical problem, FEM often leads to an overall computational advantage for both interior and exterior problems. Also, in the context of iterative solvers [e.g., generalized minimum residual (GMRES)] applicable to large-scale problems, BEM has been found to be more economical in the lower part of the problem-size range and FEM in the higher end of the scale.

For structured meshes this argument can be easily made for both two- and three-dimensional geometries. Let us consider a two-dimensional problem, with  $N_t$  points on  $\Gamma$ ,  $N_n$  points in a direction normal to  $\Gamma$ , and a nine-point stencil (corresponding to quasi-linear elements). In this case BEM leads to a matrix with  $N_t^2$  entries, whereas FEM generates a sparse matrix with  $9N_t N_n$  nonzeros. Both methods require the same amount of memory provided that  $N_t \approx 9N_n$ , which can be considered the usual situation, as shown in the preceding example on unstructured mesh. For a three-dimensional problem an equivalent discretization on  $\Gamma$  will have approximative  $N_t^2$  points, leading to  $N_t^4$  nonzeros for BEM. On the other hand, for a 27-point stencil FEM will generate a matrix with  $27N_t^2 N_n$  entries. If  $N_t^2 \approx 27N_n$ , we will have practically the same memory requirements to store the system matrix, but in general FEM can be more advantageous than BEM. The preceding argument leads to the conclusion that the domain-based approach is usually more attractive than the boundary-integral methods in terms of memory requirements.

In addition, it will be shown that the present DD approach leads to a set of smaller independent boundary-value problems, which can be solved with more accuracy and less CPU time and memory requirement.

The radiation condition (4) must be replaced by a nonreflecting condition on the outer boundary  $B$ . For example, the conventional finite element solution can be matched to an infinite element representation outside  $B$ .<sup>6</sup> Another example is the wave envelope approach, developed by Astley and Eversman,<sup>7</sup> which uses the geometrical ray theory (applicable in the high-frequency limit) to estimate the local behavior of the acoustic field. Although this local plane wave behavior does not describe the solution completely, it provides a basis for a local approximation, which is then used as part of the full numerical solution. Both methods employ special FEs to represent the far field.

In the present paper we use a conventional finite element technique with the following condition along  $B$ . If  $B$  is chosen to be a circle (in two dimensions) or a sphere (in three dimensions), an exact relation between the function and its normal derivative, called a Dirichlet-to-Neumann (DtN) map, can be derived<sup>8</sup>:

$$\frac{\partial u}{\partial n} = \mathcal{M}u \quad \text{on } B \quad (5)$$

This condition will replace Eq. (4) for the boundary-value problem in  $\Omega$ .

In two dimensions the DtN map is

$$\mathcal{M}u(R, \theta) = \frac{k}{\pi} \sum_{n=0}^{\infty} \frac{H_n^{(2)'}(kR)}{H_n^{(2)}(kR)} \int_0^{2\pi} \cos n(\theta - \theta') u(R, \theta') d\theta' \quad (6)$$

where  $R$  is the circle radius,  $H_n^{(2)}$  is the Hankel function of the second kind, and the prime on the sum indicates that the first term is halved. In practice, the sum is truncated to a finite number of terms  $N$ . Harari and Hughes<sup>9</sup> have shown that in order to guarantee the uniqueness of the solution  $N \geq kR$ . An alternative approach has been proposed by Grote and Keller,<sup>10</sup> which keeps the exact DtN for the first  $N$  modes (where  $N$  can be smaller than  $kR$ ) while using the Sommerfeld condition for the higher-order modes. It is computationally advantageous to reduce the integration interval in Eq. (6) from  $[\theta - \pi, \theta + \pi]$  to a smaller interval centered around  $\theta$  as in Refs. 11 and 12.

### III. Domain Decomposition Method

Figure 1c shows the decomposition of the computational domain into several nonoverlapping subdomains. For each subdomain  $\Omega_i$  we define a boundary-value problem at iteration  $m$ :

$$\nabla^2 u_i^m + k^2 u_i^m = 0 \quad \text{in} \quad \Omega_i \quad (7)$$

$$u_i^m = f \quad \text{on} \quad \Gamma_i \cap \Gamma_D \quad (8)$$

$$\frac{\partial u_i^m}{\partial n_i} = g \quad \text{on} \quad \Gamma_i \cap \Gamma_N \quad (9)$$

$$\frac{\partial u_i^m}{\partial n_i} + iku_i^m = \mathcal{M}u_i^{m-1} + iku_i^{m-1} \quad \text{on} \quad \mathcal{B}_i \quad (10)$$

$$\frac{\partial u_i^m}{\partial n_i} + iku_i^m = \frac{\partial u_j^{m-1}}{\partial n_i} + iku_j^{m-1} \quad \text{on} \quad \Sigma_i \quad (11)$$

where  $\Sigma_i$  are the subdomain interfaces. Because impedance-like conditions  $(\partial u_i^m / \partial n_i + iku_i^m)$  are used on the subdomain boundaries other than the physical boundary  $\Gamma$ , the subdomain solution is unique.

As shown in Fig. 1c, a subdomain  $\Omega_i$  may have only a segment  $\mathcal{B}_i$  of the outer boundary  $\mathcal{B}$ , and as a result the nonlocal condition (6) cannot be used for the subdomain problem. We avoid this difficulty by introducing the condition (10) on the outer boundary segment  $\mathcal{B}_i$ , where the DtN map is applied on the values at the preceding iteration  $u^{m-1}$ . We will refer to this approach as *explicit* implementation of the nonreflecting condition (6).

In the transmission condition (11)  $u_j^{m-1}$  denotes the solution in subdomains  $\Omega_j$  adjacent to  $\Omega_i$  at the iteration  $m-1$ . To evaluate the right-hand-side in Eq. (11), one has to compute the normal derivative  $\partial u_j^{m-1} / \partial n_i$ . This can be avoided when employing a nonoverlapping scheme as shown in Ref. 1. When an overlapping scheme is employed, the boundary operator  $\partial / \partial n + ik$  is assumed to be already implemented for the left-hand-side of Eq. (11). As a result, updating the right-hand side in Eq. (11) implies only the evaluation of the boundary operator with the values from the adjacent subdomain  $\Omega_j$  at the iteration  $m-1$ , i.e.,  $u_j^{m-1}$ . For the first iteration we choose  $(\partial u / \partial n + iku)_i^0 = 0$  on  $\Sigma_i$  and  $\mathcal{B}_i$ .

Després<sup>13</sup> has proved the convergence of the iterative scheme with Sommerfeld conditions on the outer boundary. We have extended this proof for exterior problems, when the DtN map is used on  $\mathcal{B}$ .<sup>1</sup> Because of the explicit implementation of the nonlocal DtN, the subdomain problems are independent and can be solved concurrently, one problem per processor, on a parallel computer.<sup>11,12</sup> Communication between processors is required only for updating the right-hand side in Eqs. (10) and (11).

### IV. FE Implementation of the Overlapping Domain Decomposition Scheme

To discretize the subdomain problems using FEM, we first formulate them in the variational form. With  $H^1(\Omega)$  the usual Sobolev

space, we have to find  $u_i^m \in H^1(\Omega)$ ,  $u_i^m$  satisfying Eq. (8), such that for any weighting function  $w \in H^1(\Omega)$ , with  $w = 0$  on  $\Gamma_i \cap \Gamma_D$ ,

$$\begin{aligned} & \int_{\Omega_i} (\nabla w \cdot \nabla u_i^m - k^2 w u_i^m) d\Omega + ik \int_{\mathcal{B}_i \cup \Sigma_i} w u_i^m d\Gamma \\ & - \int_{\Gamma_i \cap \Gamma_N} w g d\Gamma - \int_{\mathcal{B}_i} w (\mathcal{M}u_i^{m-1} + iku_i^{m-1}) d\Gamma \\ & - \int_{\Sigma_i} w \left( \frac{\partial u_j^{m-1}}{\partial n_i} + iku_j^{m-1} \right) d\Gamma = 0 \end{aligned} \quad (12)$$

The finite element approach employs piecewise polynomials  $\Phi$  to approximate the solution as  $u(x, y) = \sum_l u_l \Phi_l(x, y)$ . The support of a basis function  $\Phi_l$  includes only the elements adjacent to the node  $l$ . For the Galerkin method the same functions  $\Phi$  are used as weighting functions. Because of the localized support of the  $\Phi$  functions, for an interface node  $q$  the variational formulation (12) reduces to

$$\begin{aligned} & \sum_l (u_i^m)_l \int_{\Omega_i} (\nabla \Phi_q \cdot \nabla \Phi_l - k^2 \Phi_q \Phi_l) d\Omega + ik \sum_l (u_i^m)_l \\ & \times \int_{\Sigma_i} \Phi_q \Phi_l d\Gamma = \int_{\Sigma_i} \Phi_q \left( \frac{\partial u_j^{m-1}}{\partial n_i} + iku_j^{m-1} \right) d\Gamma \end{aligned} \quad (13)$$

where  $(u_i^m)_l$  are the nodal values for  $u_i^m$ , corresponding to the nodes  $l$  adjacent to (and including) the node  $q$ .

The important idea employed in the present implementation of the overlapping DD is that when updating the right-hand side in Eq. (13) for the iteration  $m+1$  one does not need to compute  $\partial u_j^{m-1} / \partial n_i$ . This is particularly important when the interface  $\Sigma_i$  has a “saw-tooth” aspect, as often is the case when partitioning unstructured meshes. The new right-hand-side value is evaluated by using the expression in the left-hand side of Eq. (13) with  $(u_j^m)_l$  replaced by  $(u_j^{m-1})_l$ . This is the only operation that requires communication among processors when a parallel computation is used. Finding the new right-hand-side entry corresponding to the interface node  $q$  simply requires the multiplication of the  $q$ th row of the system matrix with the solution vector after swapping the overlap nodal values between adjacent subdomains.

### V. Radiating Monopole

The DD algorithm, implemented as shown in the preceding section, is applied to the model problem in Fig. 2. We define the inner boundary  $\Gamma$  as an ellipse of semi-axes  $a = 2$  and  $b = 1$ . On  $\Gamma$  Neumann conditions are imposed, corresponding to a radiated monopole located at  $(-c, 0)$  with  $c = \sqrt{(a^2 - b^2)}$ . The outer boundary is a circle of radius  $R = 3$ , on which the DtN map is used as a nonreflecting condition. The following numerical results correspond to  $k = \pi$ .

The computational domain in Fig. 2 is discretized using an unstructured triangular mesh.<sup>14</sup> Then, a nonoverlapping node partitioning is performed.<sup>15</sup> Finally, for each subdomain additional interior, boundary, and transmission nodes are identified such that each node in the original partition will have a complete adjacency list. In doing so, a one-element-row overlap is built, and the new subdomain boundaries (interfaces) are defined. Figure 3 shows a four subdomains decomposition for the unstructured triangulation.

The solution accuracy is assessed using the relative error  $|u_{\text{num}} - u_{\text{an}}| / |u_{\text{an}}|$  between the numerical results  $u_{\text{num}}$  and the analytical solution  $u_{\text{an}}$ . Figure 4a shows that when using the Sommerfeld radiation condition on  $\mathcal{B}$  spurious reflections are obtained leading to relative errors up to 30%. When using the DtN map, the errors do not exceed 0.5%, as shown in Fig. 4b. Using the exact radiation condition would have given less than 0.1% discretization error.

The algorithm performance is evaluated in terms of the convergence rate and memory requirements. To quantify the convergence rate, we define the residual norm at the iteration  $m$  as  $\sum_s \|A_s^x \{u_s\}_{\text{swap}}^{m-1} - \{b_s^x\}\|$ , where  $A_s^x$  denotes the rows of the subdomain matrix  $A_s$ , corresponding to the exclusive nodes, and the sum

is performed over all subdomains. The exclusive nodes are the ones assigned to the subdomain by the nonoverlapping node partitioning. Neither  $A_s^x$  nor  $b_s^x$  are modified during the iterations. Each subdomain problem is solved using a lower-upper (LU) factorization, which is performed only once (because the subdomain matrix is unchanged during the iterations). The residual decay is presented in Fig. 5. The final level of the residual for the iterative scheme is less than the residual value, which corresponds to the global direct solver. This is because we employ a direct solver for the smaller subdomain problems, leading to a smaller subdomain residual. The convergence rate slightly decreases as the number of subdomains increases. The last column in Table 1 shows the number of iterations required to reach the same residual level as the global direct solver. As the number of subdomains increases, the subdomain problem size decreases, making each iteration cheaper.

The memory requirements are quantified by the number of nonzeros to be stored for the subdomain matrices and their LU factorization. It can be seen from Table 1 that the total amount of memory decreases as the number of subdomains increases. Moreover, when solving the subdomain problems on a parallel computer the required processor memory is significantly smaller than the direct solver memory divided by the number of processors.

## VI. Thin Airfoil in a Transverse Gust

The governing equations for linear unsteady aerodynamics and aeroacoustics are the linearized Euler equations. The flow variables, velocity  $\mathbf{V}$ , pressure  $p$ , density  $\rho$ , and entropy  $s$ , are considered to be the sum of their mean values  $\mathbf{U}$ ,  $p_0$ ,  $\rho_0$ , and  $s_0$ , and their perturbations  $\mathbf{u}$ ,  $p'$ ,  $\rho'$ , and  $s'$ , respectively. For a uniform mean flow field  $\mathbf{U} = \mathbf{i}_1 U_0$ , the linearized Euler equations reduce to

$$\frac{D_0 \rho'}{Dt} + \rho_0 \nabla \cdot \mathbf{u} = 0 \quad (14)$$

$$\rho_0 \frac{D_0 \mathbf{u}}{Dt} = -\nabla p' \quad (15)$$

$$\frac{D_0 s'}{Dt} = 0 \quad (16)$$

where  $D_0/Dt = \partial/\partial t + U_0 \partial/\partial x_1$  is the material derivative associated with the mean flow.

Consider a thin airfoil at zero angle of attack in the preceding mean flow. According to the velocity splitting theorem (Refs. 3 and 16, p. 220), the velocity perturbation can be written as the sum

**Table 1 Model problem: Influence of the number of subdomains on memory requirements and number of iterations required to reach the residual of the global direct solver**

Number of subdomains	Total nonzeros	Nonzeros per subdomain (average)	Number of iterations
1	1,011,562	1,011,562	
2	715,269	357,634	29
3	667,360	222,453	33
4	635,392	158,848	33
5	591,412	118,282	36
6	579,411	96,568	34
7	557,235	79,605	41
8	520,950	65,118	48

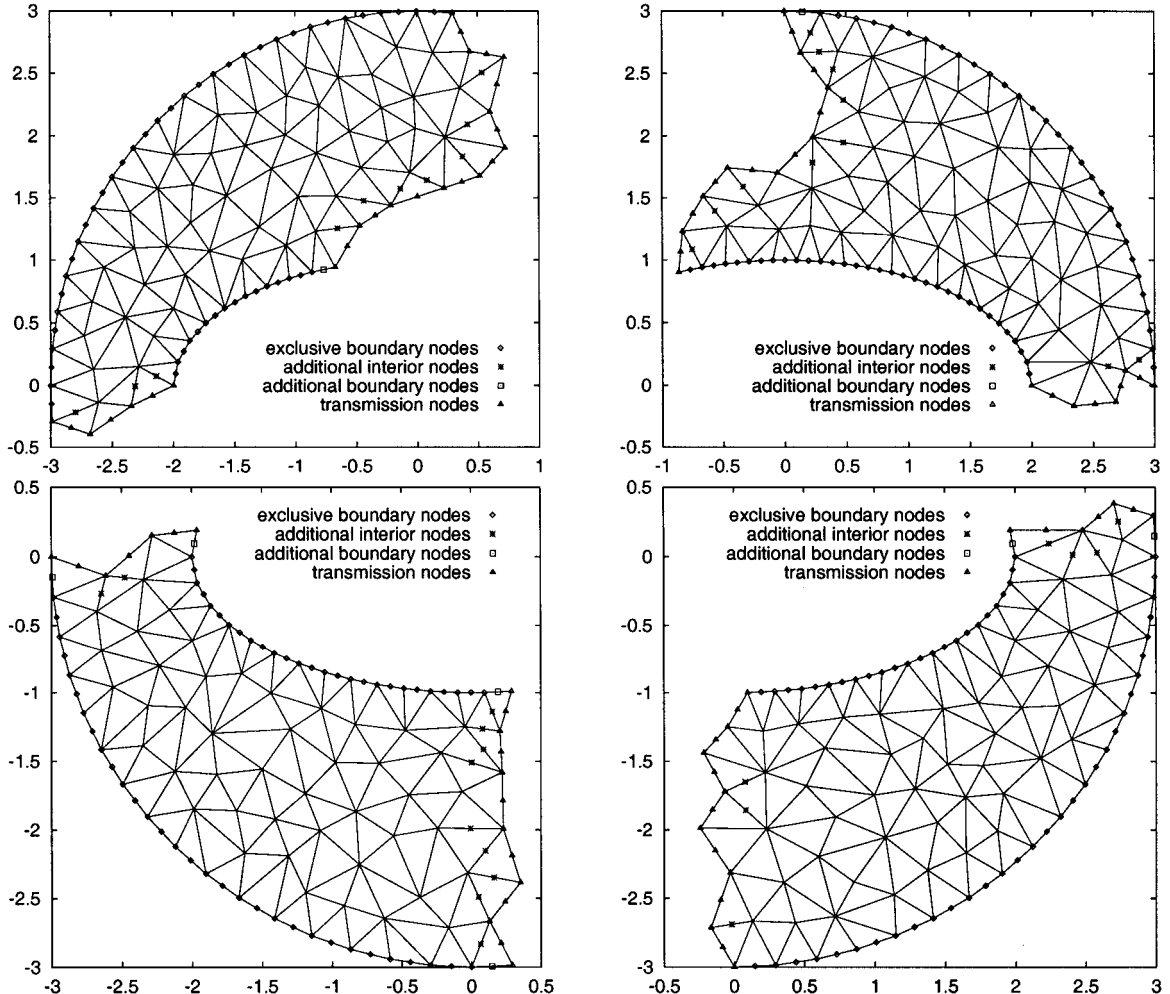


**Fig. 3 Model problem: subdomain overlapping unstructured meshes.**

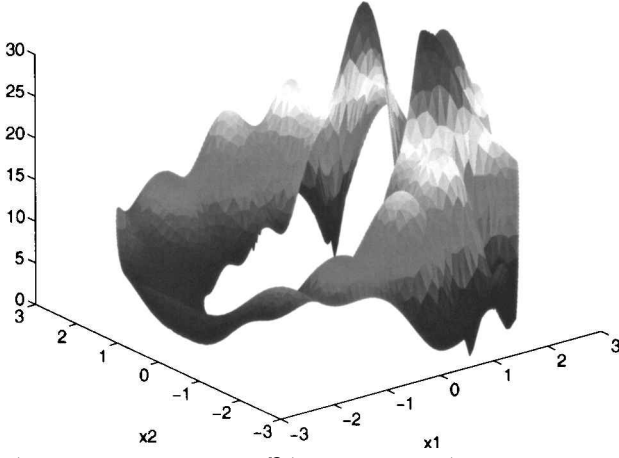
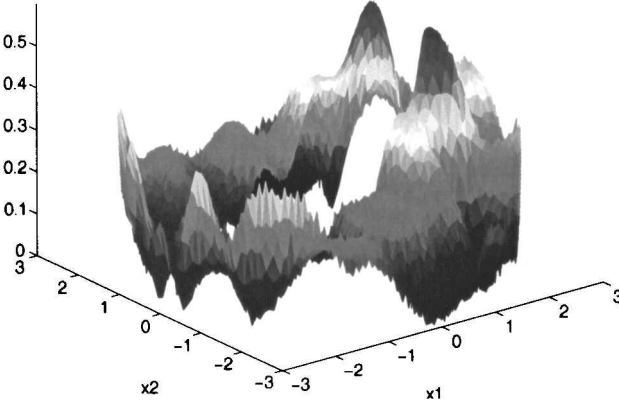
a) Sommerfeld condition on  $\mathcal{B}$  (errors up to 30%)b) DtN map on  $\mathcal{B}$  (errors less than 0.5%)

Fig. 4 Model problem: influence of the outer boundary condition on the relative error.

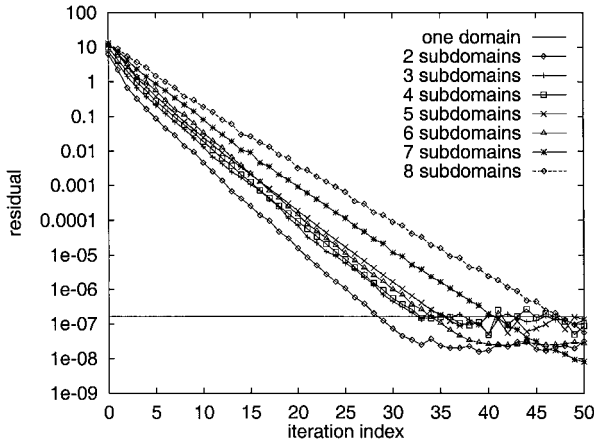


Fig. 5 Model problem: influence of the number of subdomains on the convergence rate.

$$\mathbf{u}(\mathbf{x}, t) = \mathbf{u}_v(\mathbf{x}, t) + \mathbf{u}_a(\mathbf{x}, t) \quad (17)$$

of a vortical component  $\mathbf{u}_v$  and an irrotational component  $\mathbf{u}_a$ . Here we assume no upstream incident acoustic waves. The vortical component will be divergence free  $\nabla \cdot \mathbf{u}_v = 0$ , and it will be purely convected by the mean flow  $D_0 \mathbf{u}_v / Dt = 0$ . Without loss of generality, we consider a harmonic upstream vortical disturbance (gust) of the form

$$\mathbf{u}_v = \mathbf{i}_2 a_2 \exp[i(\omega t - k_1 x_1)] \quad (18)$$

where  $\mathbf{i}_2$  is the unit vector perpendicular to the airfoil,  $a_2 \ll U_0$  is the gust amplitude,  $\omega$  is the gust angular frequency, and  $k_1 = \omega / U_0$  is the wave number.

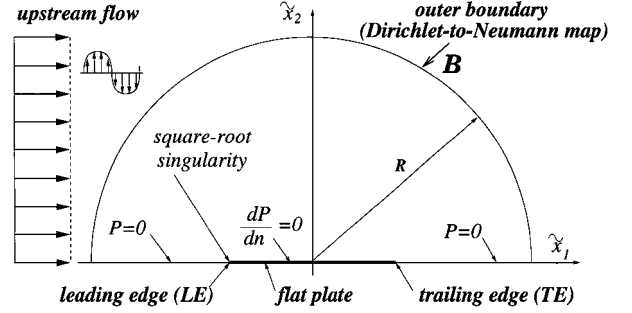


Fig. 6 Thin airfoil in a transverse gust: computational domain and boundary conditions in the Prandtl-Glauert space.

The interaction between the gust and the airfoil will produce a potential field  $\mathbf{u}_a$  governed by Eqs. (14) and (15). If we introduce the velocity potential  $\phi$ , defined by  $\mathbf{u}_a = \nabla \phi$ , we get

$$p' = -\rho_0 \frac{D\phi}{Dt} \quad (19)$$

and the convective wave equation

$$\left( \frac{D_0^2}{Dt^2} - c_0^2 \nabla^2 \right) \begin{Bmatrix} p' \\ \phi \end{Bmatrix} = 0 \quad (20)$$

where  $c_0$  is the mean-flow speed of sound. We nondimensionalize length with respect to half-chord  $c/2$ , and we introduce the reduced frequency  $k_1 = (\omega c) / (2U_0)$ . We then factor out the time dependence  $p'(\mathbf{x}, t) = \tilde{p}'(\mathbf{x}) \exp(i\omega t)$  and  $\phi(\mathbf{x}, t) = \tilde{\phi}(\mathbf{x}) \exp(i\omega t)$  and introduce the Prandtl-Glauert coordinates and the transformation

$$\tilde{x}_1 = x_1, \quad \tilde{x}_2 = x_2 \sqrt{1 - M^2}$$

$$\begin{Bmatrix} \tilde{p}' \\ \tilde{\phi} \end{Bmatrix} = \begin{Bmatrix} p' \\ \phi \end{Bmatrix} \exp(-iK_1 M x_1)$$

$$\text{with } K_1 = k_1 \frac{M}{1 - M^2}, \quad M = U_0 / c_0 \quad (21)$$

Equation (20) then reduces to the Helmholtz equation<sup>3</sup>

$$(\tilde{\nabla}^2 + K_1^2) \begin{Bmatrix} \tilde{p}' \\ \tilde{\phi} \end{Bmatrix} = 0 \quad (22)$$

Scott and Atassi<sup>17,18</sup> have solved this problem using  $\tilde{\phi}$ , which is discontinuous across the wake. In this paper as in our preliminary results,<sup>19</sup> we have chosen to solve the problem using the pressure perturbation. To this end, we introduce the dimensionless variable  $P = \tilde{p}' / (\rho_0 U_0 a_2)$ . Because the pressure field is antisymmetric with respect to  $\tilde{x}_2$ , we have chosen as a computational domain a half-circle in the upper-half-plane. Figure 6 shows the computational domain and the boundary conditions in the Prandtl-Glauert plane. On the plate the normal velocity vanishes; therefore, we have homogeneous Neumann conditions for the pressure  $\partial P / \partial n = 0$ . On the  $\tilde{x}_1$  axis upstream the leading edge (LE) and downstream the trailing edge (TE) we have homogeneous Dirichlet conditions  $P = 0$ . Finally, on the outer boundary  $\mathcal{B}$  we impose the nonreflecting boundary conditions (5).

So far, the stated boundary conditions for  $P$  are homogeneous. However, at the LE the pressure has a square-root singularity whose strength is unknown yet. We impose a unit strength singularity at the LE (as shown next) and find a unit solution  $P^{(1)}$ . The solution of the problem is thus defined up to a multiplicative constant, i.e.,  $P = C P^{(1)}$ .

#### A. Determination of the Multiplicative Constant

The constant  $C$  is found by integrating the momentum equation for the acoustic velocity ( $\mathbf{u}_a = \mathbf{i}_1 u_a + \mathbf{i}_2 v_a$ ) component normal to the plate  $v_a$  along the stagnation streamline from far upstream to the LE. This momentum equation can be written as

$$\frac{\partial}{\partial x_1} [v_a \exp(ik_1 x_1)] = -\frac{1}{\rho_0 U_0} \frac{\partial \tilde{p}'}{\partial x_2} \exp(ik_1 x_1) \quad (23)$$

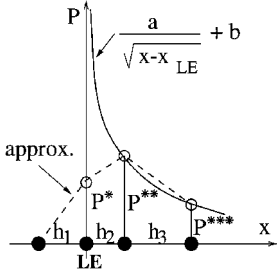


Fig. 7 LE singularity.

Noting that  $v_a \exp(ik_1 x_1)|_{x_1 \rightarrow -\infty} = 0$  and  $v_a \exp(ik_1 x_1)|_{x_1(LE)} = -1 = -a_2$ , integration of Eq. (23) yields

$$1 = C \int_{-R}^{-1} \sqrt{1 - M^2} \frac{\partial P^{(1)}}{\partial \tilde{x}_2} \exp \left[ i \left( \frac{K_1}{M} \right) \tilde{x}_1 \right] d\tilde{x}_1 \quad (24)$$

The error caused by the truncation of the integration domain from  $(-\infty, -1]$  to  $[-R, -1]$  is  $\mathcal{O}(R^{-3/2})$ .

Because of the singular behavior of  $P$  near the LE, the local flux  $F_g$  is used in evaluating Eq. (24), with smaller elements near LE,

$$1 = C \sqrt{1 - M^2} \sum_g F_g \exp \left[ i \left( \frac{K_1}{M} \right) \tilde{x}_{1g} \right] \quad (25)$$

where  $g$  denotes the index of the nodes on the integration line.

### B. Numerical Approximation for the LE Singularity

We assume a piecewise linear interpolation for  $P$  along the  $x_1$  axis. Figure 7 shows the analytical behavior (solid curve) of the pressure on the plate near the LE and its numerical approximation (dot line).

We seek a relationship between the values  $P^*$ ,  $P^{**}$ , and  $P^{***}$  such that the piecewise linear approximation reflects the average behavior of the square-root singularity. To this end, we impose the following conditions:

1) The integral around the LE should be the same:

$$2a\sqrt{h_2 + h_3 + b(h_2 + h_3)} = \frac{1}{2}P^*h_1 + \frac{1}{2}(P^* + P^{**})h_2 + \frac{1}{2}(P^{**} + P^{***})h_3 \quad (26)$$

2) The derivative near the LE should be the same:

$$-\{a/[2(h_2 + h_3/2)^{3/2}]\} = (P^{***} - P^{**})/h_3 \quad (27)$$

3) The value near the LE should be the same:

$$a/\sqrt{h_2} + b = P^{**} \quad (28)$$

After eliminating the unknown constants  $a$  and  $b$ , we obtain the following relationship:

$$\alpha_1 P^* + \alpha_2 P^{**} + \alpha_3 P^{***} = 0 \quad (29)$$

where

$$\begin{aligned} \alpha_1 &= \frac{h_1 + h_2}{h_2 + h_3} \\ \alpha_2 &= -1 - \frac{4(h_2 + h_3/2)^{3/2}}{h_3} \left( \frac{2}{\sqrt{h_2 + h_3}} - \frac{1}{\sqrt{h_2}} \right) \\ \alpha_3 &= \frac{h_3}{h_2 + h_3} + \frac{4(h_2 + h_3/2)^{3/2}}{h_3} \left( \frac{2}{\sqrt{h_2 + h_3}} - \frac{1}{\sqrt{h_2}} \right) \end{aligned}$$

The unit solution  $P^{(1)}$  is obtained by imposing  $P^{**} = 1.0$ .

### C. Numerical Results

The computational domain is decomposed into two overlapping subdomains as shown in Fig. 8. After discretizing the boundary-value problem for each subdomain, one obtains the systems of equations  $[A_i]\{P_i\} = \{b_i\}$ ,  $i = 1, 2$ . LU factorization of  $[A_i]$  is performed for each subdomain.

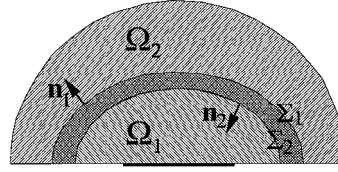


Fig. 8 Thin airfoil problem: two overlapping subdomains decomposition.

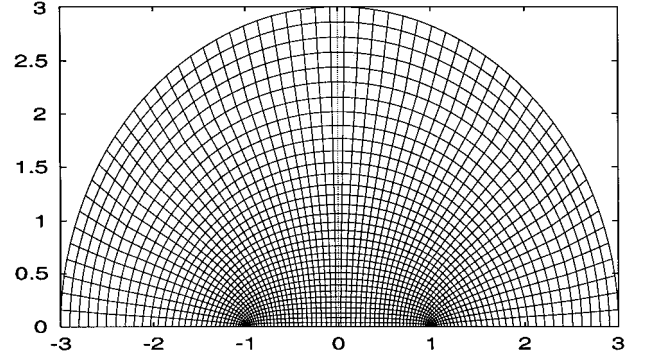


Fig. 9 Thin airfoil problem: finite element structured mesh.

#### 1. Accuracy

The FE mesh used for the present computations is shown in Fig. 9. We have used quadrilateral four-noded elements and structured mesh with 2100 nodes.

Figure 10 shows a comparison between results for the dimensionless pressure  $\tilde{P}'/(\rho_0 U_0 a_2)$  obtained with the present method and those obtained by solving the Possio<sup>20</sup> singular integral equation. An excellent agreement is observed for different Mach numbers.

For the far field we use the Green's theorem to express  $P$  in terms of its value along the airfoil:<sup>2</sup>

$$P(\tilde{x}) = \frac{-i}{4} K_1 \tilde{x}_2 \int_{-1}^1 \Delta P(\tilde{y}_1) \frac{H_1^{(2)}(K_1 \tilde{r})}{\tilde{r}} d\tilde{y}_1 \quad (30)$$

where  $\tilde{y} = (\tilde{y}_1, 0)$  denotes a point on the airfoil,  $\tilde{r} = |\tilde{x} - \tilde{y}|$ , and  $\Delta P(\tilde{y}_1) = 2P(\tilde{y}_1)$  is the pressure jump across the airfoil. Figure 11 presents the directivity,  $\sqrt{(r)}|\tilde{P}'|/(\rho_0 U_0 a_2)$ , computed using the pressure values on the outer boundary  $B$ . Once again, our results agree very well with those obtained by employing the integral representation (30).

If one is interested in finding the acoustic pressure beyond the computational domain, our results can be easily extrapolated. This is possible because the outer boundary in the Prandtl-Glauert space is a circle with the following analytical solution for the exterior Helmholtz problem:

$$P(\theta, \tilde{r}) = \frac{1}{\pi} \sum_{n=0}^{\infty} \frac{H_n^{(2)}(K_1 \tilde{r})}{H_n^{(2)}(K_1 R)} \int_0^{2\pi} \cos n(\theta - \theta') P(R, \theta') d\theta' \quad (31)$$

where  $\tilde{r} \geq R$  stands here for  $|\tilde{x}|$ .

#### 2. Convergence

The convergence of the DD iterative scheme is investigated using the residual defined as in Sec. V. Figure 12 presents the convergence rate for two values of the Mach number. First, it can be seen that the convergence rate is improved by increasing the overlap. Second, the convergence rate decreases as the Mach number (and consequently  $K_1$  for  $k_1$  fixed) decreases. These observations confirm that the convergence rate is in fact determined by the so-called wavelap.<sup>21</sup> If  $\delta$  quantifies the width of the overlapping region, we take  $K_1 \delta$  as a measure of the wavelap.

For our computations the iterations were stopped when the residual does not decay anymore. In practice, one cannot need to decrease the residual by 10 orders of magnitude, and the iterations can be stopped earlier. An acceleration method, such as GMRES, can be used with the present algorithm as a preconditioner to significantly

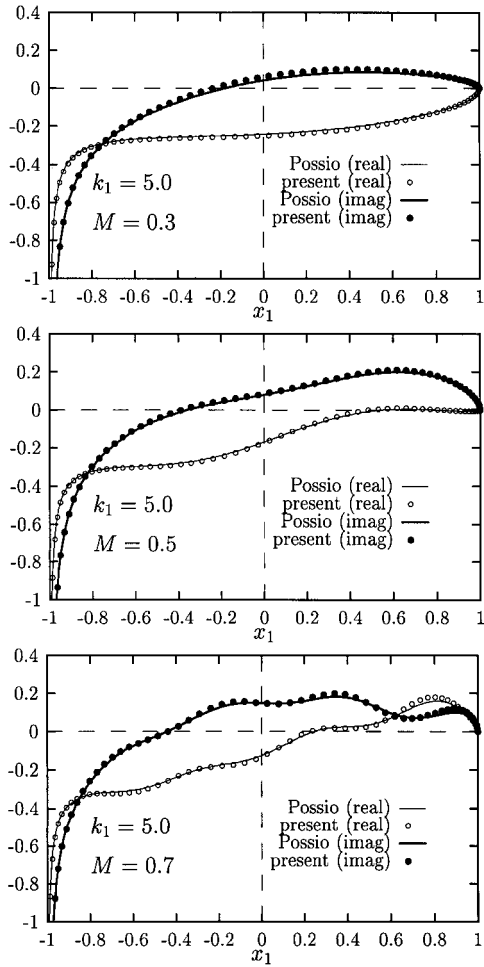


Fig. 10 Dimensionless pressure  $\tilde{p}/(\rho_0 U_0 a_2)$  on the thin airfoil subject to a transverse gust.

enhance the convergence rate. Such a technique is currently under implementation.

3. Computation Time and Memory Requirements

The main goal of a DD algorithm is to reduce the computation time and memory requirements for large-scale systems.

For our numerical experiments we have used a direct solver [from the International Mathematical and Statistical Library (IMSL), with sparse matrix storage and LU factorization] for both the whole domain and the subdomains. The memory requirements are quantified by the number of nonzero complex values to be stored (corresponding to the system matrix and its factorization), and the computing time corresponds to an IBM-RISC6000 workstation. Of course, the real amount of memory used is a bit larger, including the overhead for sparse matrix storage and the working vectors, and the computing time is larger than the actual CPU time. However, here we are interested in quantifying the benefits of the DD method in comparison with the single-domain approach.

Table 2 presents the computing time and number of nonzeros obtained for our problem, with the mesh from Fig. 9. The DD algorithm by reducing the size of the matrices substantially reduces both the assembling and the factorization times. Also, the total number of nonzeros is reduced to approximately one-half, even if the number of unknowns has been slightly increased because of the overlap. The iteration time, introduced by the DD, can be significantly decreased by increasing the overlap. Therefore, even when the algorithm is used for a single-processor machine, just by using the DD with two subdomains one can reduce to almost one-half both the computing time and the memory requirements. When using a parallel computer, the subdomain matrices are assembled and factorized concurrently on different processors. The performances of this DD algorithm on parallel computers are investigated in Refs. 11 and 12 for a simple exterior Helmholtz problem.

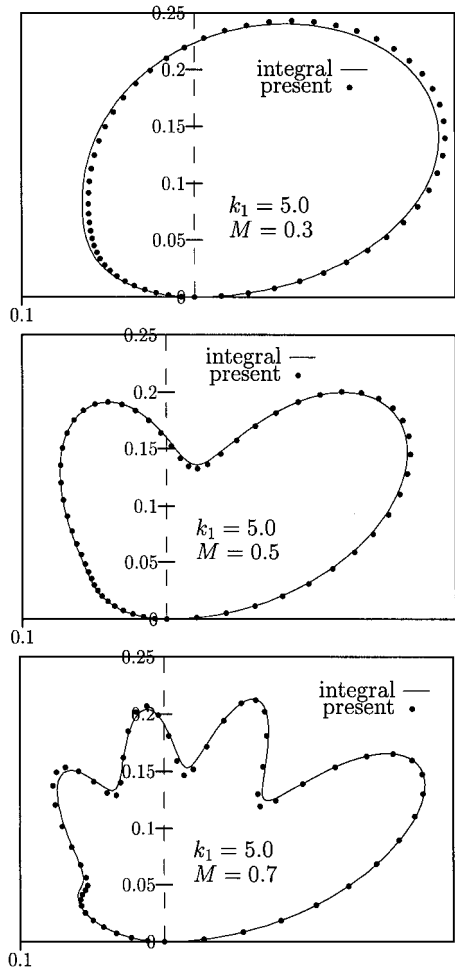


Fig. 11 Acoustic radiation from a thin airfoil subject to a transverse gust: polar plot of the directivity  $\sqrt{r}| \tilde{p}|/l(\rho_0 U_0 a_2)$ .

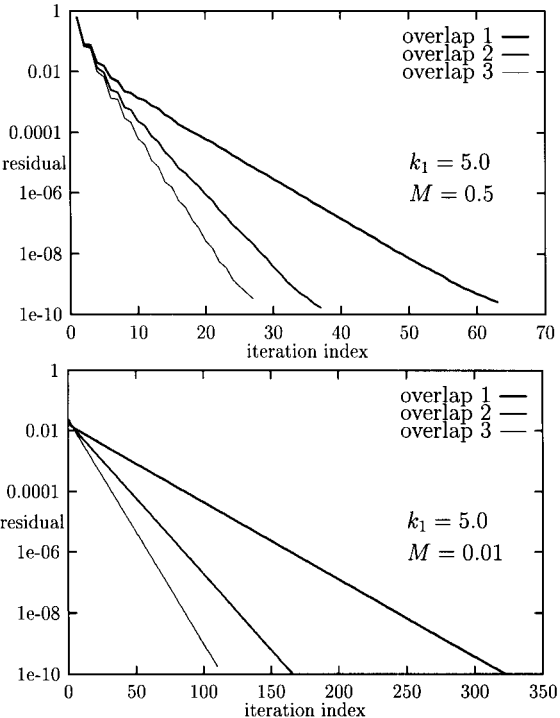


Fig. 12 Thin airfoil problem: influence of the overlap on the convergence rate.

**Table 2 Thin airfoil problem: Influence of the overlap on computing time and memory requirements (reduced frequency  $k_1 = 5.0$  and Mach number  $M = 0.5$ )**

Parameter	One domain	Overlap 1		Overlap 2		Overlap 3	
		$\Omega_1$	$\Omega_2$	$\Omega_1$	$\Omega_2$	$\Omega_1$	$\Omega_2$
Nodes	2,100	1,140	1,080	1,200	1,080	1,260	1,080
Matrix nonzeros	21,181	9,605	12,276	10,129	12,276	10,653	12,276
Assembling time, s	93	23	29	25	29	25	29
Factorization nonzeros	233,703	59,232	70,748	67,195	70,748	68,902	70,748
Factorization time, s	38	10	11	11	11	11	11
Number of iterations			63		37		27
Iteration time, s			27		16		12

## VII. Conclusions

This paper presents a domain-based formulation for time-harmonic radiation and scattering problems. The nonreflecting condition on the outer boundary of the computational domain uses an exact nonlocal Dirichlet-to-Neumann map.

A domain-decomposition method is employed to solve the boundary-value problem in the computational domain. On the artificial subdomain interfaces we introduce impedance-like transmission conditions to ensure subdomain solution uniqueness. The DD iterative scheme employs an explicit implementation of the Dirichlet-to-Neumann map. The subdomain problems are independent and can be solved concurrently on a parallel computer.

Each subdomain problem is discretized with finite elements. The computation of the normal derivatives on the subdomain interfaces is avoided by using a subdomain overlap, which is particularly advantageous when saw-tooth interfaces are obtained as a result of unstructured mesh partitioning. Updating the interface conditions involves only swapping the interface nodal values between adjacent subdomains, therefore minimizing the communication between processors when parallel computing is used.

For a model problem corresponding to a radiating monopole, we present an overlapping DD on unstructured meshes. The accuracy of the numerical solution is investigated in comparison with the analytical solution, and the importance of correct nonreflecting conditions on the outer boundary is emphasized. We present the influence of the number of subdomains on the convergence rate, as well as on the memory requirements. It is shown that when solving the subdomain problems on a parallel computer the required processor memory is significantly smaller than the global direct solver memory divided by the number of processors.

The DD algorithm is then applied to a model aeroacoustic problem, corresponding to a thin airfoil in a transverse gust. We formulate the boundary-value problem for the unsteady pressure to avoid the velocity discontinuity across the wake and use the Dirichlet-to-Neumann map as a nonreflecting condition on the outer boundary. A two subdomain decomposition is used on a structured mesh, and the effect of the overlap on the iterative scheme performance is investigated. It is shown that by increasing the overlap the convergence rate can be significantly improved. The memory requirements and the computation time are substantially reduced compared to a direct global solver, making the present algorithm suitable for both single-processor and parallel computers.

## Acknowledgment

This research was supported by the National Science Foundation under Grant NSF-ECS-9527169.

## References

- <sup>1</sup>Susan-Resiga, R. F., and Atassi, H. M., "A Domain Decomposition Method for the Exterior Helmholtz Problem," *Journal of Computational Physics*, Vol. 147, 1998, pp. 388–401.
- <sup>2</sup>Atassi, H. M., Dusey, M., and Davis, C. M., "Acoustic Radiation from a Thin Airfoil in Nonuniform Subsonic Flow," *AIAA Journal*, Vol. 31, No. 1, 1993, pp. 12–19.
- <sup>3</sup>Atassi, H. M., "Unsteady Aerodynamics of Vortical Flows: Early and Recent Developments," *Aerodynamics and Aeroacoustics*, edited by K. Y. Fung, World Scientific, Singapore, 1994, pp. 121–171.

<sup>4</sup>Ihlenburg, F., *Finite Element Analysis of Acoustic Scattering*, Springer-Verlag, New York, 1998, Chap. 3.

<sup>5</sup>Harari, I., and Hughes, T. J. R., "A Cost Comparison of Boundary Element and Finite Element Methods for Problems of Time-Harmonic Acoustics," *Computer Methods in Applied Mechanics and Engineering*, Vol. 97, 1992, pp. 77–102.

<sup>6</sup>Bettess, P., "Infinite Elements," *International Journal for Numerical Methods in Engineering*, Vol. 11, 1977, pp. 53–64.

<sup>7</sup>Astley, R. J., and Eversman, W., "Wave Envelope Elements for Acoustical Radiation in Inhomogeneous Media," *Computers and Structures*, Vol. 30, No. 4, 1988, pp. 801–810.

<sup>8</sup>Keller, J. B., and Givoli, D., "Exact Non-Reflecting Boundary Conditions," *Journal of Computational Physics*, Vol. 82, 1989, pp. 172–192.

<sup>9</sup>Harari, I., and Hughes, T. J. R., "Analysis of Continuous Formulations Underlying the Computation of Time-Harmonic Acoustics in Exterior Domains," *Computer Methods in Applied Mechanics and Engineering*, Vol. 97, 1992, pp. 103–124.

<sup>10</sup>Grote, M. J., and Keller, J. B., "On Nonreflecting Boundary Conditions," *Journal of Computational Physics*, Vol. 122, 1995, pp. 231–243.

<sup>11</sup>McInnes, L. C., Susan-Resiga, R. F., Atassi, H. M., and Keyes, D. E., "Additive Schwarz Methods with Nonreflecting Boundary Conditions for the Parallel Computation of Helmholtz Problems," *Domain Decomposition Methods 10*, edited by J. Mandel, C. Farhat, and X.-C. Cai, No. 218, Contemporary Mathematics, American Mathematical Society, Providence, RI, 1998, pp. 325–333.

<sup>12</sup>McInnes, L. C., Susan-Resiga, R. F., Keyes, D. E., and Atassi, H. M., "Parallel Solution of Helmholtz Problems Using Additive Schwarz Methods," *Mathematical and Numerical Aspects of Wave Propagation*, edited by J. A. DeSanto, Society for Industrial and Applied Mathematics, Philadelphia, 1998, pp. 623–625.

<sup>13</sup>Després, B., "Décomposition de Domaine et Problème de Helmholtz," *Comptes Rendus de l'Académie des Sciences*, Vol. 311, 1990, pp. 313–316.

<sup>14</sup>Shewchuk, J. R., "Triangle: Engineering a 2D Quality Mesh Generator and Delaunay Triangulator," *Applied Computational Geometry: Towards Geometric Engineering*, edited by M. C. Lin and D. Manocha, Vol. 1148, Lecture Notes in Computer Science, Springer-Verlag, New York, 1996, pp. 203–222.

<sup>15</sup>Karypis, G., and Kumar, V., "Fast and High Quality Multilevel Scheme for Partitioning Irregular Graphs," *SIAM Journal on Scientific Computing*, Vol. 20, No. 1, 1998, pp. 359–392.

<sup>16</sup>Goldstein, M. E., *Aeroacoustics*, McGraw-Hill, New York, 1976, p. 220.

<sup>17</sup>Scott, J. R., and Atassi, H. M., "A Finite Difference Frequency-Domain Numerical Scheme for the Solution of the Linearized Euler Equations," *Computational Fluid Dynamics Symposium on Aeropropulsion*, NASA CP-10045, 1990, Chap. 5, pp. 1–50.

<sup>18</sup>Scott, J. R., and Atassi, H. M., "A Finite Difference Frequency Domain Numerical Scheme for Solution of the Gust Response Problem," *Journal of Computational Physics*, Vol. 119, 1995, pp. 75–93.

<sup>19</sup>Susan-Resiga, R. F., and Atassi, H. M., "Parallel Computing Using Schwarz Domain Decomposition Method for Aeroacoustic Problems," *Proceedings of the 4th AIAA/CEAS Aeroacoustics Conference*, Vol. 1, AIAA, Reston, VA, 1998, pp. 86–96; also AIAA Paper 98-2218, June 1998.

<sup>20</sup>Possio, C., "L'Azione Aerodinamica sul Profilo Oscillante in un Fluido Compressibile a Velocità Iposonora," *L'Aerotecnica*, Vol. 18, No. 4, 1938.

<sup>21</sup>Cai, X.-C., Casarin, M. A., Elliot, F. W., and Widlund, O. B., "Overlapping Schwarz Algorithms for Solving Helmholtz's Equation," *Domain Decomposition Methods 10*, edited by J. Mandel, C. Farhat, and X.-C. Cai, No. 218, Contemporary Mathematics, American Mathematical Society, Providence, RI, 1998, pp. 391–399.